Surrogate Assisted Design of Spline-Based Ogive Radome

M. Salucci, G. Oliveri, M. A. Hannan and A. Massa

Contents

1 Design 2 - "wide training bounds" ($t_i \in [0.2\lambda_r, 0.8\lambda_r]$)

1.1 Analysis of the training set (LHS, $N = 250$)

This section reports the results of the simulations performed in order to analyze the accuracy of the Kriging-based predictor with different correlation models.

1.1.1 Parameters

Optimization targets

- Number of variables: $K = 5$;
- Frequency range:
  - Minimum frequency: $f_{min} = 10.75$ $[GHz]$;
  - Maximum frequency: $f_{max} = 14.5$ $[GHz]$;
  - Number of frequency steps: $N_f = 10$ ($\Delta f \simeq 0.42$ $[GHz]$);
  - Central frequency: $f_0 = \frac{f_{min}+f_{max}}{2} \simeq 12.63$ $[GHz]$;
  - Free-space wavelength at the central frequency: $\lambda_0 = \frac{c}{f_0} = 2.38 \times 10^{-2}$ $[m]$;
- Scanning angle range:
  - Minimum scanning angle: $\theta_{min} = 0$ $[deg]$;
  - Maximum scanning angle: $\theta_{max} = 45$ $[deg]$;
  - Number of angular steps: $N_\theta = 4$ ($\theta_1 = 0$ $[deg]$, $\theta_2 = 15$ $[deg]$, $\theta_3 = 30$ $[deg]$, $\theta_4 = 45$ $[deg]$);

Kriging (Gaussian Process Regressor) parameters

- Regression model: constant (Ordinary Kriging);
- Correlation models:
  - Exponential ($p = 1$);
  - Gaussian ($p = 2$);
- Initial guess for hyper-parameters θ_h: $\theta_{h,0} = 0.5$, for $h = 1, ..., K$;
- Lower bound for hyper-parameters θ_h: $min\{\theta_h\} = 0.1$, for $h = 1, ..., K$;
- Upper bound for hyper-parameters θ_h: $max\{\theta_h\} = 20.0$, for $h = 1, ..., K$;

Incremental training parameters

- Number of available simulations: $S = 250$ (LHS sampling);

- Dimension of the training sets: $N_1 = 20$, $N_{max} = N_L = 200$, step $\Delta N = 20$;

Not-optimized (static) radome parameter

Parameter	Description	Value
L	Length of the radome	1.59×10^{-1} $[m] \simeq 6.69$ λ_0
D	Base diameter of the radome	1.27×10^{-1} $[m] \simeq 5.35$ λ_0
t_0	Thickness of the base and of the top of the radome	$8.20 \times 10^{-3}[m] \simeq \frac{\lambda_r}{2}$
z_1	z-coordinate of the spline control point 1	$\frac{L-t_0}{6}$
z_2	z-coordinate of the spline control point 2	$2\frac{L-t_0}{6}$
z_3	z-coordinate of the spline control point 3	$3\frac{L-t_0}{6}$
z_4	z-coordinate of the spline control point 4	$4\frac{L-t_0}{6}$
z_5	z-coordinate of the spline control point 5	$5\frac{L-t_0}{6}$
ν	External curvature of the radome ($\nu \in [1, 2]$)	1.449 (tangent ogive)
ε_r	Permittivity of the radome material	2.10 (Teflon)
tanδ_r	Tangent delta of the radome material	$tan\delta = 3.00 \times 10^{-4}$ @ 10.0 $[GHz]$ (Teflon)
λ_r	Wavelength in the radome material	$\lambda_r \simeq \frac{c}{f_0\sqrt{\varepsilon}} \simeq 1.64 \times 10^{-1}$[m]

Table I: List of non-optimized radome parameters.

Antenna Parameters

- Linear dipole array placed over circular ground plane (PEC).
- Number of array elements: $N_e = 8$
- Dipole length: $l_e = \frac{\lambda_0}{2}$
- Array elements spacing: $d_e = \lambda/2$
- Spacing between the array and the ground plane: $h_e = \frac{\lambda_0}{4}$

Parameters boundaries

Parameter	Description	Min	Max
t_1	Radome thickness at the quota $z = z_1$	3.28×10^{-3} [m] $(0.2\lambda_r)$	13.12×10^{-3} [m] $(0.8\lambda_r)$
t_2	Radome thickness at the quota $z = z_2$	3.28×10^{-3} [m] $(0.2\lambda_r)$	13.12×10^{-3} [m] $(0.8\lambda_r)$
t_3	Radome thickness at the quota $z = z_3$	3.28×10^{-3} [m] $(0.2\lambda_r)$	13.12×10^{-3} [m] $(0.8\lambda_r)$
t_4	Radome thickness at the quota $z = z_4$	3.28×10^{-3} [m] $(0.2\lambda_r)$	13.12×10^{-3} [m] $(0.8\lambda_r)$
t_5	Radome thickness at the quota $z = z_5$	3.28×10^{-3} [m] $(0.2\lambda_r)$	13.12×10^{-3} [m] $(0.8\lambda_r)$

Table II: List of all considered boundaries for the optimized radome descriptors.

1.1.2 Analysis of the training set

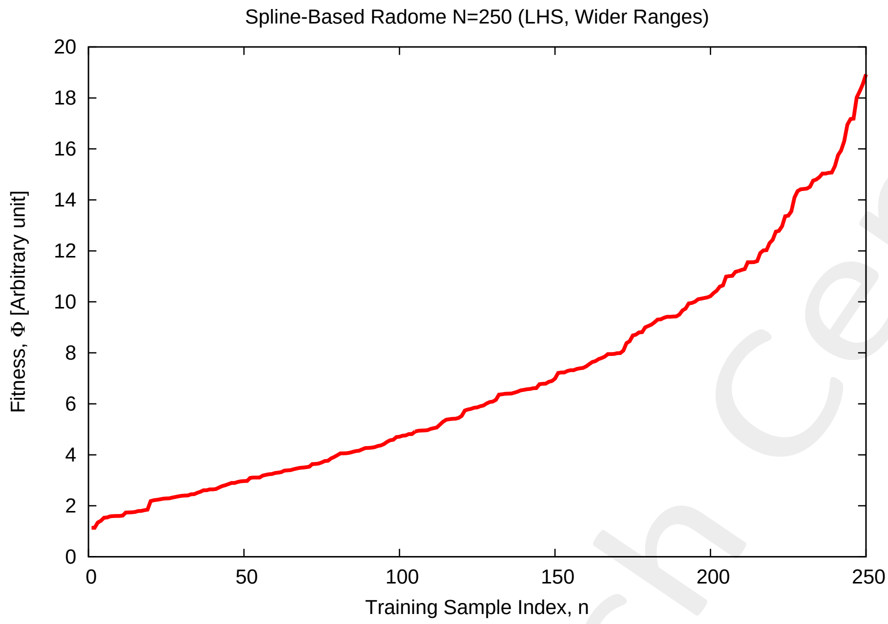

Figure 1: Fitness value computed for each training sample (sorted in ascending order).

- Best fitness in the training set: $\Phi_{train}^{opt} = 1.13$;
- Worst fitness in the training set: $\Phi_{train}^{worst} = 18.93$.

1.1.3 Predicted Fitness Values

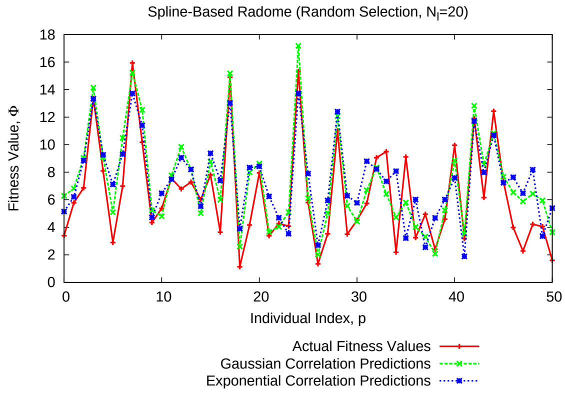

(a) $N = 20$

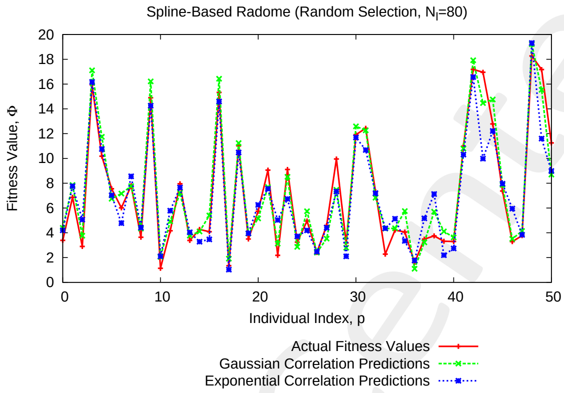

(b) $N = 80$

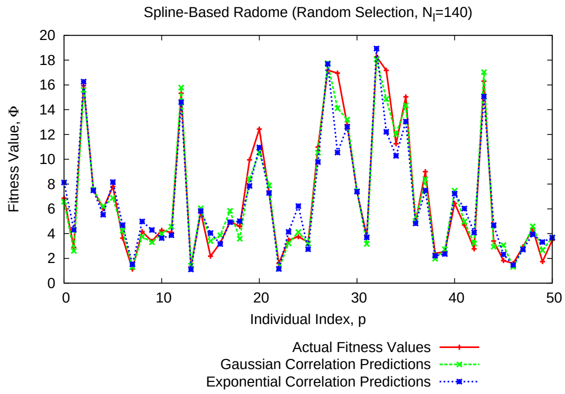

(c) $N = 140$

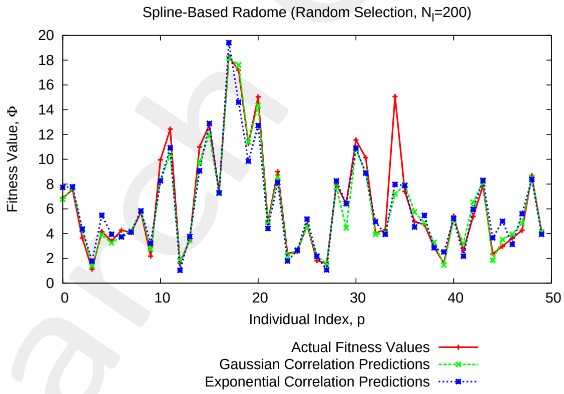

(d) $N = 200$

Figure 2: Actual and predicted functional values of 50 random individuals for different training sizes (N): (a) $N = 20$, (b) $N = 80$, (c) $N = 140$ and (d) $N = 200$.

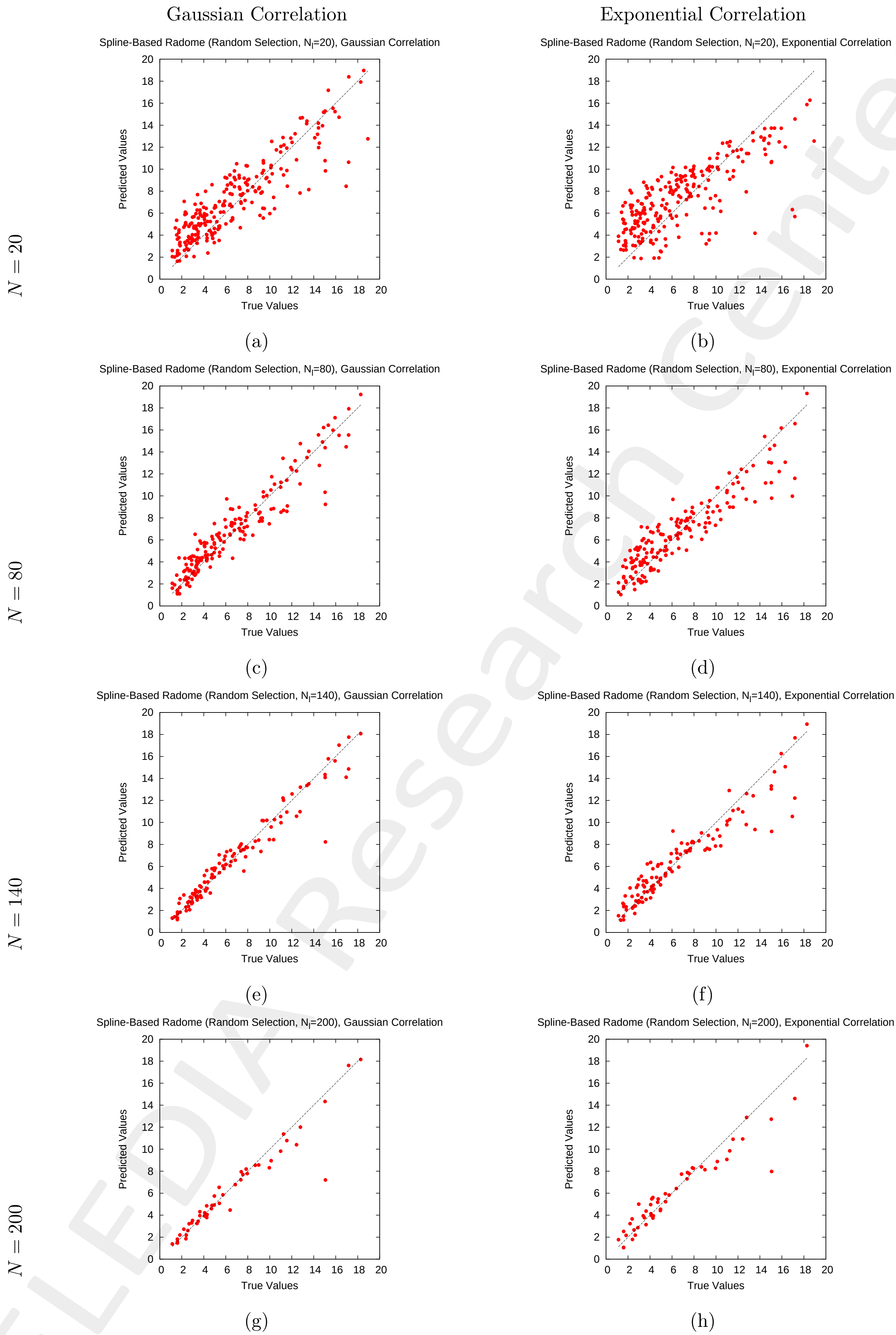

Figure 3: Plot of predicted vs actual values for (a), (c), (e), (g) Gaussian Correlation Model and (b), (d), (f), (h) Exponential Correlation Model for different training sizes (N): (a),(b) $N = 20$, (c),(d) $N = 80$, (e),(f) $N = 140$ and (g),(h) $N = 200$.

1.1.4 Prediction error vs. training size

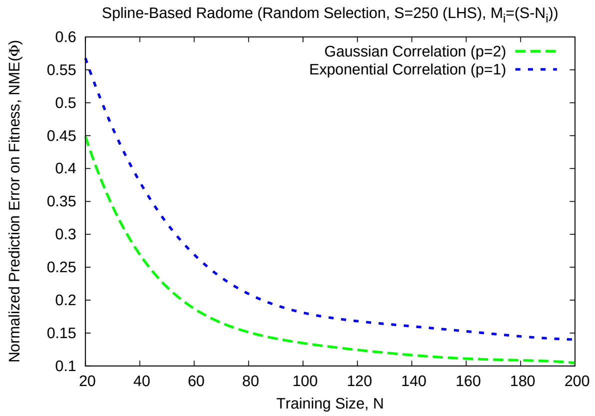

(a) NME

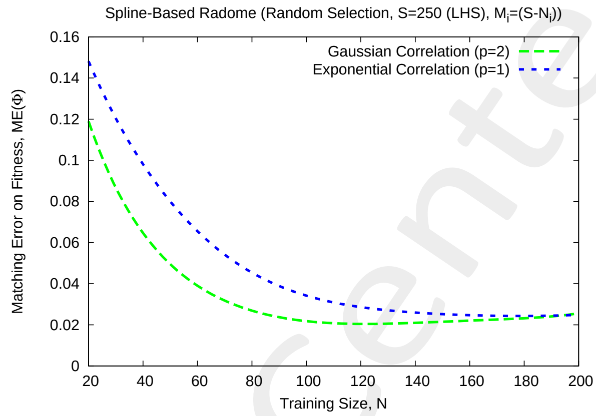

(b) ME

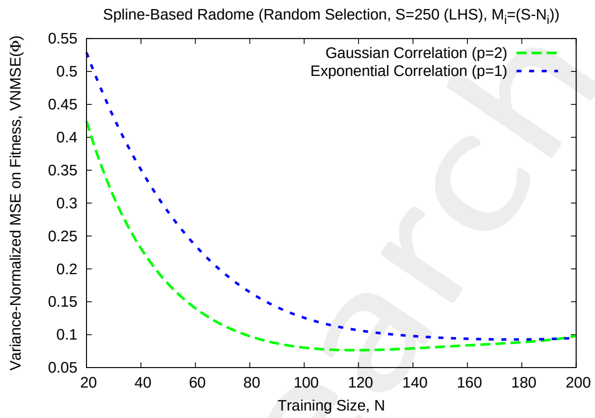

(c) $VNMSE$

Figure 4: Prediction errors vs. training size (N) when considering an incremental training with random selection of N training samples form a set of $S = 250$ available simulations (LHS. Each time the trained Kriging model is tested on a test set made by the remaining $M = (S - N)$ simulations.

		Gaussian Correlation			**Exponential Correlation**		
N	M	NME	ME	$VNMSE$	NME	ME	$VNMSE$
20	230	3.53×10^{-1}	6.52×10^{-2}	4.25×10^{-1}	5.44×10^{-1}	1.27×10^{-1}	5.29×10^{-1}
80	170	1.94×10^{-1}	2.78×10^{-2}	7.08×10^{-2}	2.70×10^{-1}	4.74×10^{-2}	1.13×10^{-1}
140	110	1.13×10^{-1}	1.65×10^{-2}	8.09×10^{-2}	1.80×10^{-1}	3.38×10^{-2}	9.99×10^{-2}
200	50	9.77×10^{-2}	2.82×10^{-2}	9.81×10^{-2}	1.71×10^{-1}	3.25×10^{-2}	9.50×10^{-2}

Table III: Prediction errors vs. training size (N).

1.1.5 Prediction error vs. time saving

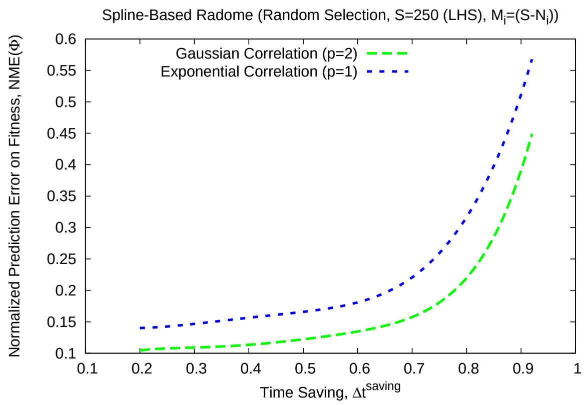

(a) NME

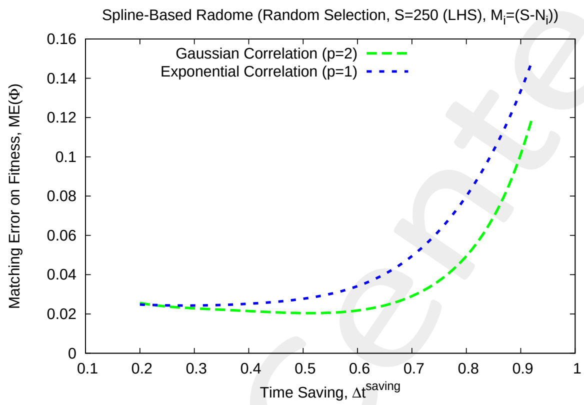

(b) ME

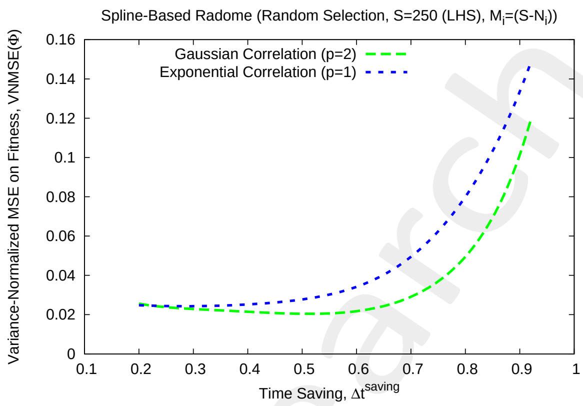

(c) $VNMSE$

Figure 5: Prediction errors vs. Time Saving (Δt^{saving}) when considering an incremental training with random selection of N training samples form a set of $S = 250$ available simulations (LHS. Each time the trained Kriging model is tested on a test set made by the remaining $M = (S - N)$ simulations.

1.1.6 Prediction errors and time saving vs. training size

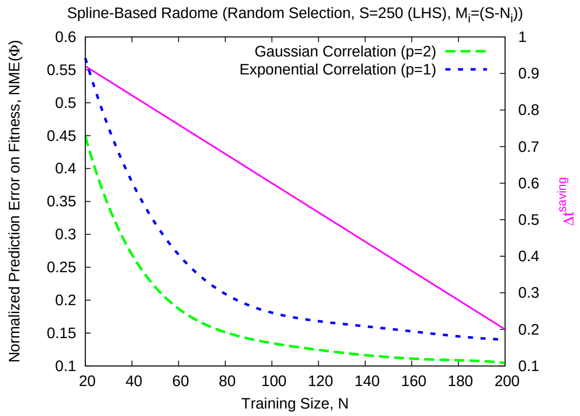

(a) NME

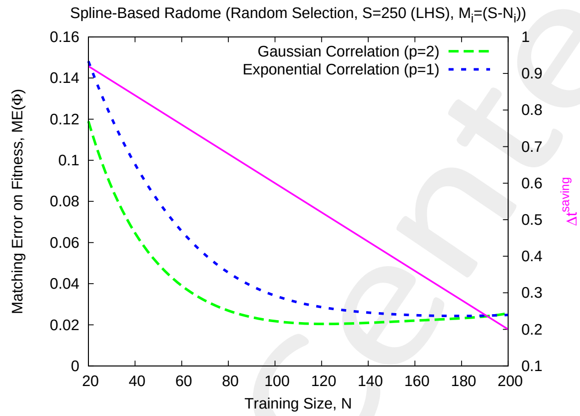

(b) ME

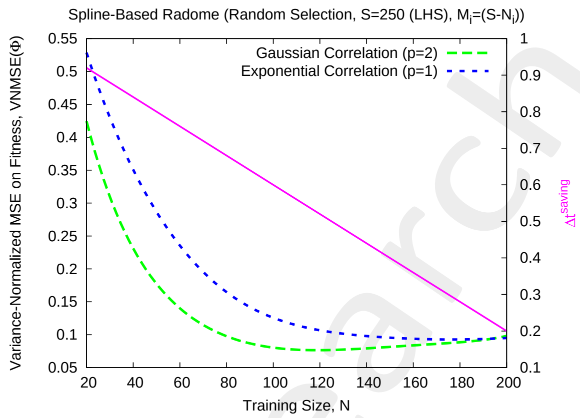

(c) $VNMSE$

Figure 6: Prediction errors and time saving vs. training size (N) when considering an incremental training with random selection of N training samples form a set of $S = 250$ available simulations (LHS. Each time the trained Kriging model is tested on a test set made by the remaining $M = (S - N)$ simulations.

1.1.7 Comparative assessment (Narrow Bounds vs. Wide Bounds Training)

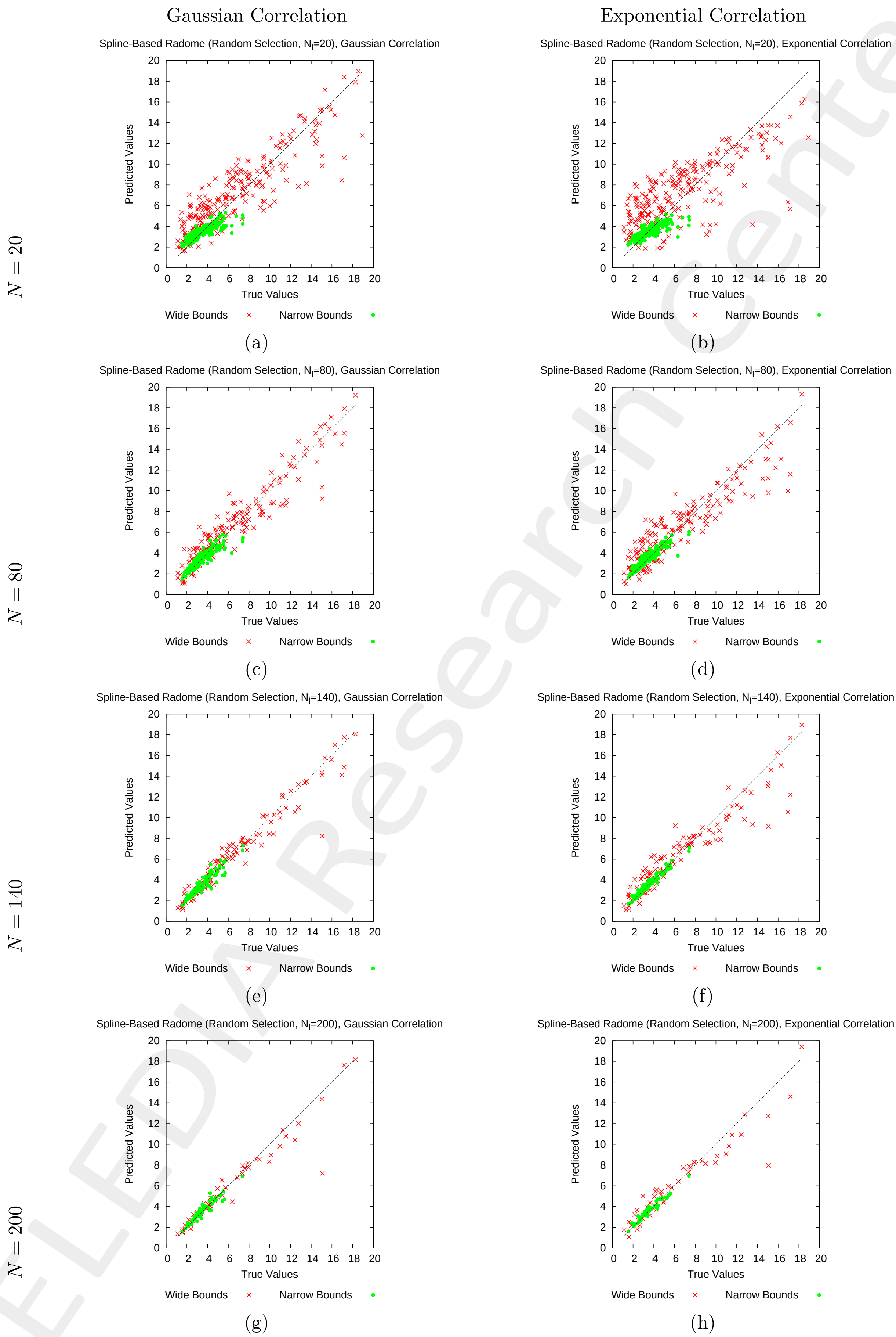

Figure 7: Plot of predicted vs actual values for (a), (c), (e), (g) Gaussian Correlation Model and (b), (d), (f), (h) Exponential Correlation Model for different training sizes (N): (a),(b) $N = 20$, (c),(d) $N = 80$, (e),(f) $N = 140$ and (g),(h) $N = 200$.

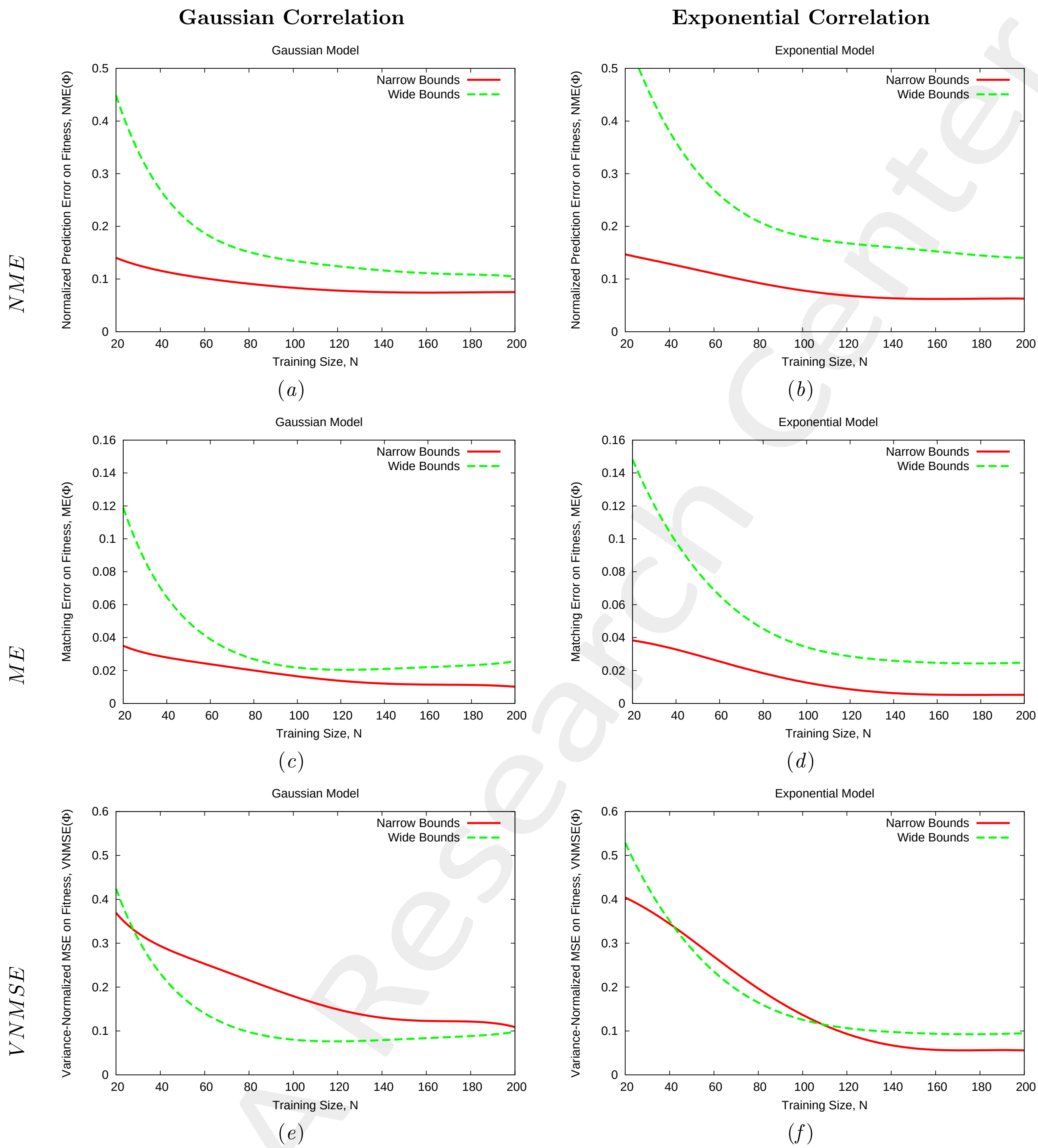

Figure 8: Plot of (a) Normalized Mean Error (NME) and (b) Matching Error (ME) vs training size (N) when considering an incremental training with random selection of N_l training samples form a set of S available simulations and testing the corresponding Kriging model on a test set made by the remaining $M_l = (S - N_l)$ simulations.

1.2 Optimization with PSO+Kriging (no update during optimization)

1.2.1 Parameters

Optimization targets

- Number of variables: $K = 5$;
- Frequency range:
  - Minimum frequency: $f_{min} = 10.75$ $[GHz]$;
  - Maximum frequency: $f_{max} = 14.5$ $[GHz]$;
  - Number of frequency steps: $N_f = 10$ ($\Delta f \simeq 0.42$ $[GHz]$);
  - Central frequency: $f_0 = \frac{f_{min}+f_{max}}{2} \simeq 12.63$ $[GHz]$;
  - Free-space wavelength at the central frequency: $\lambda_0 = \frac{c}{f_0} = 2.38 \times 10^{-2}$ $[m]$;
- Scanning angle range:
  - Minimum scanning angle: $\theta_{min} = 0$ $[deg]$;
  - Maximum scanning angle: $\theta_{max} = 45$ $[deg]$;
  - Number of angular steps: $N_\theta = 4$ ($\theta_1 = 0$ $[deg]$, $\theta_2 = 15$ $[deg]$, $\theta_3 = 30$ $[deg]$, $\theta_4 = 45$ $[deg]$);

PSO **parameters**

- Population dimension: $P = 10$;
- Maximum number of iterations: $I_{max} = 200$;
- Fitness threshold: $\Phi^{th} = 10^{-20}$;
- Inertial weight: $w = 0.4$;
- Constant inertial velocity;
- Exploration coefficient: $c_1 = 2$;
- Exploitation coefficient: $c_2 = 2$;
- Random seed $S = 1, 2, ..., 10$;

Kriging (Gaussian Process Regressor) parameters

- Regression model: constant (Ordinary Kriging);
- Correlation models:
  - Exponential ($p = 1$);

- Initial guess for hyper-parameters θ_h: $\theta_{h,0} = 0.5$, for $h = 1, ..., K$;
- Lower bound for hyper-parameters θ_h: $min\{\theta_h\} = 0.1$, for $h = 1, ..., K$;
- Upper bound for hyper-parameters θ_h: $max\{\theta_h\} = 20.0$, for $h = 1, ..., K$;

Not-optimized (static) radome parameter

Parameter	Description	Value
L	Length of the radome	1.59×10^{-1} $[m] \simeq 6.69$ λ_0
D	Base diameter of the radome	1.27×10^{-1} $[m] \simeq 5.35$ λ_0
t_0	Thickness of the base and of the top of the radome	$8.20 \times 10^{-3}[m] \simeq \frac{\lambda_r}{2}$
z_1	z-coordinate of the spline control point 1	$\frac{L-t_0}{6}$
z_2	z-coordinate of the spline control point 2	$2\frac{L-t_0}{6}$
z_3	z-coordinate of the spline control point 3	$3\frac{L-t_0}{6}$
z_4	z-coordinate of the spline control point 4	$4\frac{L-t_0}{6}$
z_5	z-coordinate of the spline control point 5	$5\frac{L-t_0}{6}$
ν	External curvature of the radome ($\nu \in [1, 2]$)	1.449 (tangent ogive)
ε_r	Permittivity of the radome material	2.10 (Teflon)
$\tan\delta_r$	Tangent delta of the radome material	$tan\delta = 3.00 \times 10^{-4}$ @ 10.0 $[GHz]$ (Teflon)
λ_r	Wavelength in the radome material	$\lambda_r \simeq \frac{c}{f_0\sqrt{\varepsilon}} \simeq 1.64 \times 10^{-1}$

Table IV: List of non-optimized radome parameters.

Antenna Parameters

- Linear dipole array placed over circular ground plane (PEC)
- Number of array elements: $N_e = 8$
- Dipole length: $l_e = \frac{\lambda_0}{2}$
- Array elements spacing: $d_e = \lambda/2$
- Spacing between the array and the ground plane: $h_e = \frac{\lambda_0}{4}$

Parameters boundaries

Parameter	Description	Min	Max
t_1	Radome thickness at the quota $z = z_1$	3.28×10^{-3}[m] $(0.2\lambda_r)$	13.12×10^{-3}[m] $(0.8\lambda_r)$
t_2	Radome thickness at the quota $z = z_2$	3.28×10^{-3}[m] $(0.2\lambda_r)$	13.12×10^{-3}[m] $(0.8\lambda_r)$
t_3	Radome thickness at the quota $z = z_3$	3.28×10^{-3}[m] $(0.2\lambda_r)$	13.12×10^{-3}[m] $(0.8\lambda_r)$
t_4	Radome thickness at the quota $z = z_4$	3.28×10^{-3}[m] $(0.2\lambda_r)$	13.12×10^{-3}[m] $(0.8\lambda_r)$
t_5	Radome thickness at the quota $z = z_5$	3.28×10^{-3}[m] $(0.2\lambda_r)$	13.12×10^{-3}[m] $(0.8\lambda_r)$

Table V: List of all considered boundaries for the optimized radome descriptors.

1.2.2 Results of the optimization (seed 1,...,10) - Exponential Correlation Model

- Number of performed PSO iterations: $I_{tot} = I = 200$ for every seed.
- Total number of simulations: $E = \tau = 250$ (only for training).
- Final value of the fitness (predicted and actual):

	Predicted			Actual	
Seed	$\widehat{\Phi}^{init}$	$\widehat{\Phi}^{opt}$	$\left\lvert\frac{\widehat{\Phi}^{opt}}{\widehat{\Phi}^{init}}\right\rvert$	Φ^{opt}	$100\frac{\Phi^{opt}_{train}-\Phi^{opt}}{\Phi^{opt}_{train}}$
1	2.80	-4.33×10^{-1}	6.48	1.35	-1.87×10^{1}
2	1.12	-4.88×10^{-1}	2.29	1.62	-4.30×10^{1}
3	1.18	-6.71×10^{-1}	1.76	1.32	-1.59×10^{1}
4	2.28	-6.11×10^{-1}	3.73	1.52	-3.43×10^{1}
5	1.26	-5.93×10^{-1}	2.13	1.55	-3.70×10^{1}
6	1.32	-4.52×10^{-1}	2.92	1.25	-1.01×10^{1}
7	1.96	-6.88×10^{-1}	2.85	1.32	-1.59×10^{1}
8	2.73	-4.35×10^{-1}	6.27	1.16	-2.49
9	1.35	-4.88×10^{-1}	2.76	1.62	-4.30×10^{1}
10	4.20	-4.88×10^{-1}	8.62	1.62	-4.30×10^{1}

Table VI: Final value of the predicted and actual fitness values ($\widehat{\Phi}^{init}$ is the initial predicted fitness, $\widehat{\Phi}^{opt}$ is the optimal predicted fitness, Φ^{opt} is the optimal actual fitness and $\Phi^{opt}_{train} = 1.13$ is the best individual in the training set).

Figure 9: Predicted and actual fitness values vs seed. The lowest training sample is equal to $\Phi^{opt}_{train} = 1.13$.

1.2.3 Results of the optimization (seed 1,...,10) - Gaussian Correlation Model

- Number of performed PSO iterations: $I_{tot} = I = 200$ for every seed.
- Total number of simulations: $E = \tau = 250$ (only for training).
- Final value of the fitness (predicted and actual):

	Predicted			Actual	
Seed	$\widehat{\Phi}^{init}$	$\widehat{\Phi}^{opt}$	$\left\lvert\frac{\widehat{\Phi}^{opt}}{\widehat{\Phi}^{init}}\right\rvert$	Φ^{opt}	$100\frac{\Phi^{opt}_{train}-\Phi^{opt}}{\Phi^{opt}_{train}}$
1	3.05	-6.32×10^{-1}	2.07×10^{-1}	1.19	-4.70
2	1.91	5.40×10^{-2}	2.83×10^{-2}	2.07	-8.25×10^{1}
3	2.26	-6.32×10^{-1}	2.80×10^{-1}	1.18	-4.20
4	1.67	-6.32×10^{-1}	3.77×10^{-1}	1.18	-4.37
5	1.50	5.40×10^{-2}	3.60×10^{-2}	2.07	-8.25×10^{1}
6	1.82	5.40×10^{-2}	2.97×10^{-2}	2.07	-8.25×10^{1}
7	2.24	-6.32×10^{-1}	2.82×10^{-1}	1.19	-4.72
8	3.49	5.40×10^{-2}	1.55×10^{-2}	2.07	-8.25×10^{1}
9	1.58	-6.32×10^{-1}	3.99×10^{1}	1.19	-4.82
10	3.29	-6.32×10^{-1}	1.92×10^{-1}	1.19	-4.82

Table VII: Final value of the predicted and actual fitness values ($\widehat{\Phi}^{init}$ is the initial predicted fitness, $\widehat{\Phi}^{opt}$ is the optimal predicted fitness, Φ^{opt} is the optimal actual fitness and $\Phi^{opt}_{train} = 1.13$ is the best individual in the training set).

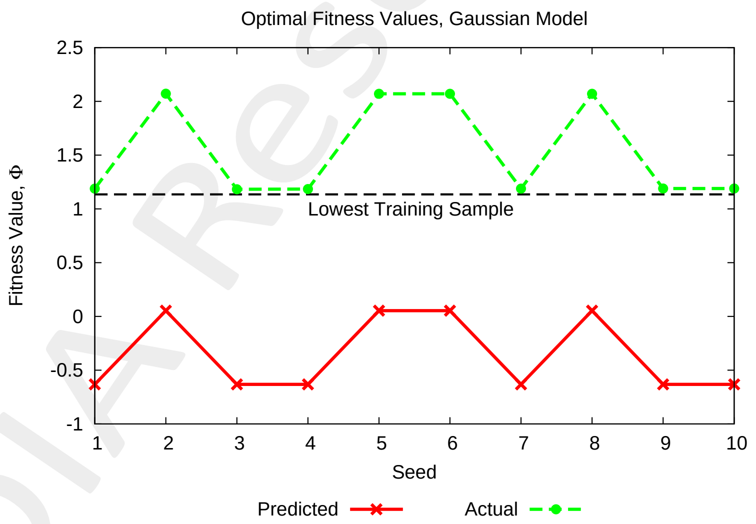

Figure 10: Predicted and actual fitness values vs seed. The lowest training sample is equal to $\Phi^{opt}_{train} = 1.13$.

1.2.4 Results of the optimization (seed 1,...,10) - Exponential Correlation Model (model re-trained in the locations where the the predicted fitness is negative)

The results reported in this section have been obtained by training the predictor using the actual solutions computed for the analysis in Sections (1.2.2) and (1.2.3). The objective of this additional training is to avoid negative predicted fitness values.

- Number of performed PSO iterations: $I_{tot} = I = 200$ for every seed.
- Total number of simulations: $E = \tau = 270$ (only for training).
- Final value of the fitness (predicted and actual):

	Predicted			Actual	
Seed	$\widehat{\Phi}^{init}$	$\widehat{\Phi}^{opt}$	$\frac{\widehat{\Phi}^{opt}}{\widehat{\Phi}^{init}}$	Φ^{opt}	$100\frac{\Phi^{opt}_{train}-\Phi^{opt}}{\Phi^{opt}_{train}}$
1	2.75	2.18×10^{-1}	7.95×10^{-2}	1.26	-1.07×10^{1}
2	1.21	1.54×10^{-1}	1.28×10^{-1}	1.28	-1.29×10^{1}
3	1.61	1.31×10^{-1}	8.16×10^{-2}	1.07	5.80
4	2.30	1.40×10^{-1}	6.09×10^{-2}	1.18	-4.13
5	1.63	1.94×10^{-1}	1.19×10^{-1}	1.33	-1.73×10^{1}
6	1.28	1.94×10^{-1}	1.52×10^{-1}	1.33	-1.68×10^{1}
7	1.88	3.78×10^{-1}	2.01×10^{-1}	8.55×10^{-1}	2.47×10^{1}
8	3.02	1.94×10^{-1}	6.43×10^{-2}	1.33	-1.72×10^{1}
9	1.59	2.23×10^{-1}	1.40×10^{-2}	1.09	3.87
10	4.28	1.22×10^{-1}	2.85×10^{-2}	1.24	-9.08

Table VIII: Final value of the predicted and actual fitness values ($\widehat{\Phi}^{init}$ is the initial predicted fitness, $\widehat{\Phi}^{opt}$ is the optimal predicted fitness, Φ^{opt} is the optimal actual fitness and $\Phi^{opt}_{train} = 1.13$ is the best individual in the training set).

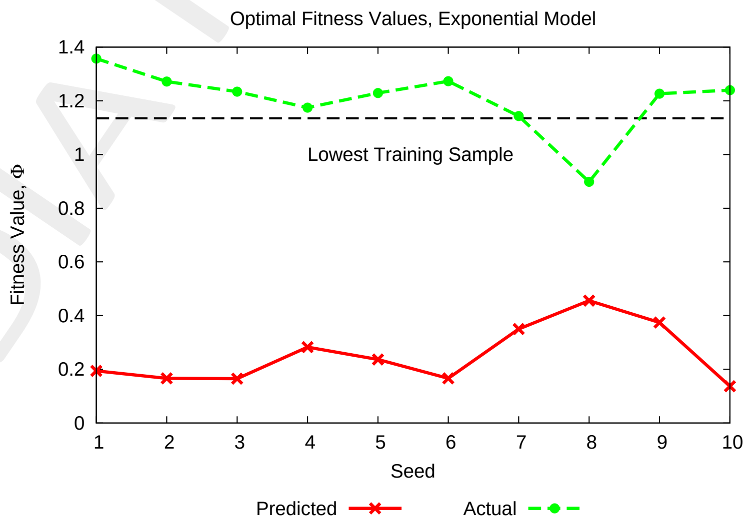

Figure 11: Predicted and actual fitness values vs seed. The lowest training sample is equal to $\Phi^{opt}_{train} = 1.13$.

More information on the topics of this document can be found in the following list of references.

References

[1] A. Massa, D. Marcantonio, X. Chen, M. Li, and M. Salucci, "DNNs as applied to electromagnetics, antennas, and propagation - A review," *IEEE Antennas and Wirel. Propag. Lett.,* vol. 18, no. 11, pp. 2225-2229, Nov. 2019.

[2] A. Massa, G. Oliveri, M. Salucci, N. Anselmi, and P. Rocca, "Learning-by-examples techniques as applied to electromagnetics," *Journal of Electromagnetic Waves and Applications, Invited Review Article*, pp. 1-16, 2017.

[3] G. Oliveri, M. Salucci, and A. Massa, "Towards reflectarray digital twins - An EM-driven machine learning perspective," *IEEE Trans. Antennas Propag. - Special Issue on 'Machine Learning in Antenna Design, Modeling, and Measurements'*, vol. 70, no. 7, pp. 5078-5093, July 2022.

[4] M. Salucci, L. Tenuti, G. Oliveri, and A. Massa, "Efficient prediction of the EM response of reflectarray antenna elements by an advanced statistical learning method," *IEEE Trans. Antennas Propag.*, vol. 66, no. 8, pp. 3995-4007, Aug. 2018.

[5] M. Salucci, G. Oliveri, M. A. Hannan, and A. Massa, "System-by-design paradigm-based synthesis of complex systems: The case of spline-contoured 3D radomes," *IEEE Antennas and Propagation Magazine - Special Issue on 'Artificial Intelligence in Electromagnetics,'*, vol. 64, no. 1, pp. 72-83, Feb. 2022.

[6] G. Oliveri, P. Rocca, M. Salucci, and A. Massa, "Holographic smart EM skins for advanced beam power shaping in next generation wireless environments," *IEEE J. Multiscale Multiphysics Comput. Tech.*, vol. 6, pp. 171-182, Oct. 2021.

[7] G. Oliveri, A. Gelmini, A. Polo, N. Anselmi, and A. Massa, "System-by-design multi-scale synthesis of task-oriented reflectarrays," *IEEE Trans. Antennas Propag.*, vol. 68, no. 4, pp. 2867-2882, Apr. 2020.

[8] M. Salucci, L. Tenuti, G. Gottardi, A. Hannan, and A. Massa, "System-by-design method for efficient linear array miniaturisation through low-complexity isotropic lenses" *Electronic Letters*, vol. 55, no. 8, pp. 433-434, May 2019.

[9] M. Salucci, N. Anselmi, S. Goudos, and A. Massa, "Fast design of multiband fractal antennas through a system-by-design approach for NB-IoT applications," *EURASIP J. Wirel. Commun. Netw.*, vol. 2019, no. 1, pp. 68-83, Mar. 2019.

[10] M. Salucci, G. Oliveri, N. Anselmi, and A. Massa, "Material-by-design synthesis of conformal miniaturized linear phased arrays," *IEEE Access*, vol. 6, pp. 26367-26382, 2018.

[11] M. Salucci, G. Oliveri, N. Anselmi, G. Gottardi, and A. Massa, “Performance enhancement of linear active electronically-scanned arrays by means of MbD-synthesized metalenses," *Journal of Electromagnetic Waves and Applications*, vol. 32, no. 8, pp. 927-955, 2018.

[12] G. Oliveri, M. Salucci, N. Anselmi and A. Massa, “Multiscale System-by-Design synthesis of printed WAIMs for waveguide array enhancement," *IEEE J. Multiscale Multiphysics Computat. Techn.*, vol. 2, pp. 84-96, 2017.

[13] A. Massa and G. Oliveri, “Metamaterial-by-Design: Theory, methods, and applications to communications and sensing - Editorial," *EPJ Applied Metamaterials*, vol. 3, no. E1, pp. 1-3, 2016.

[14] G. Oliveri, F. Viani, N. Anselmi, and A. Massa, “Synthesis of multi-layer WAIM coatings for planar phased arrays within the system-by-design framework," *IEEE Trans. Antennas Propag.*, vol. 63, no. 6, pp. 2482-2496, June 2015.

[15] G. Oliveri, L. Tenuti, E. Bekele, M. Carlin, and A. Massa, “An SbD-QCTO approach to the synthesis of isotropic metamaterial lenses" *IEEE Antennas Wireless Propag. Lett.*, vol. 13, pp. 1783-1786, 2014.

[16] A. Massa, G. Oliveri, P. Rocca, and F. Viani, “System-by-Design: a new paradigm for handling design complexity," *8th European Conference on Antennas Propag. (EuCAP 2014), The Hague, The Netherlands*, pp. 1180-1183, Apr. 6-11, 2014.

[17] P. Rocca, M. Benedetti, M. Donelli, D. Franceschini, and A. Massa, “Evolutionary optimization as applied to inverse problems," *Inverse Problems - 25 th Year Special Issue of Inverse Problems, Invited Topical Review*, vol. 25, pp. 1-41, Dec. 2009.

[18] P. Rocca, G. Oliveri, and A. Massa, “Differential Evolution as applied to electromagnetics," *IEEE Antennas Propag. Mag.*, vol. 53, no. 1, pp. 38-49, Feb. 2011.

[19] P. Rocca, N. Anselmi, A. Polo, and A. Massa, “Pareto-optimal domino-tiling of orthogonal polygon phased arrays," *IEEE Trans. Antennas Propag.*, vol. 70, no. 5, pp. 3329-3342, May 2022.

[20] P. Rocca, N. Anselmi, A. Polo, and A. Massa, “An irregular two-sizes square tiling method for the design of isophoric phased arrays," *IEEE Trans. Antennas Propag.*, vol. 68, no. 6, pp. 4437-4449, Jun. 2020.

[21] P. Rocca, N. Anselmi, A. Polo, and A. Massa, “Modular design of hexagonal phased arrays through diamond tiles," *IEEE Trans. Antennas Propag.*, vol.68, no. 5, pp. 3598-3612, May 2020.

[22] N. Anselmi, L. Poli, P. Rocca, and A. Massa, “Design of simplified array layouts for preliminary experimental testing and validation of large AESAs," *IEEE Trans. Antennas Propag.*, vol. 66, no. 12, pp. 6906-6920, Dec. 2018.

[23] N. Anselmi, P. Rocca, M. Salucci, and A. Massa, “Contiguous phase-clustering in multibeam-on-receive scanning arrays," *IEEE Trans. Antennas Propag.*, vol. 66, no. 11, pp. 5879-5891, Nov. 2018.

[24] G. Oliveri, G. Gottardi, F. Robol, A. Polo, L. Poli, M. Salucci, M. Chuan, C. Massagrande, P. Vinetti, M. Mattivi, R. Lombardi, and A. Massa, "Co-design of unconventional array architectures and antenna elements for 5G base station," *IEEE Trans. Antennas Propag.*, vol. 65, no. 12, pp. 6752-6767, Dec. 2017.

[25] N. Anselmi, P. Rocca, M. Salucci, and A. Massa, "Irregular phased array tiling by means of analytic schemata-driven optimization," *IEEE Trans. Antennas Propag.*, vol. 65, no. 9, pp. 4495-4510, Sept. 2017.

[26] N. Anselmi, P. Rocca, M. Salucci, and A. Massa, "Optimization of excitation tolerances for robust beamforming in linear arrays" *IET Microwaves, Antennas & Propagation*, vol. 10, no. 2, pp. 208-214, 2016.

[27] P. Rocca, R. J. Mailloux, and G. Toso, "GA-Based optimization of irregular sub-array layouts for wideband phased arrays desig," *IEEE Antennas and Wireless Propag. Lett.*, vol. 14, pp. 131-134, 2015.

[28] P. Rocca, M. Donelli, G. Oliveri, F. Viani, and A. Massa, "Reconfigurable sum-difference pattern by means of parasitic elements for forward-looking monopulse radar," *IET Radar, Sonar & Navigation*, vol 7, no. 7, pp. 747-754, 2013.

[29] P. Rocca, L. Manica, and A. Massa, "Ant colony based hybrid approach for optimal compromise sum-difference patterns synthesis," *Microwave Opt. Technol. Lett.*, vol. 52, no. 1, pp. 128-132, Jan. 2010.

[30] P. Rocca, L. Manica, and A. Massa, "An improved excitation matching method based on an ant colony optimization for suboptimal-free clustering in sum-difference compromise synthesis," *IEEE Trans. Antennas Propag.*, vol. 57, no. 8, pp. 2297-2306, Aug. 2009.

[31] N. Anselmi, L. Poli, P. Rocca, and A. Massa, "Design of simplified array layouts for preliminary experimental testing and validation of large AESAs," *IEEE Trans. Antennas Propag.*, vol. 66, no. 12, pp. 6906-6920, Dec. 2018.

[32] M. Salucci, F. Robol, N. Anselmi, M. A. Hannan, P. Rocca, G. Oliveri, M. Donelli, and A. Massa, "S-Band spline-shaped aperture-stacked patch antenna for air traffic control applications," *IEEE Trans. Antennas Propag.*, vol. 66, no. 8, pp. 4292-4297, Aug. 2018.

[33] F. Viani, F. Robol, M. Salucci, and R. Azaro, "Automatic EMI filter design through particle swarm optimization," *IEEE Trans. Electromagnet. Compat.*, vol. 59, no. 4, pp. 1079-1094, Aug. 2017.